INTERNATIONAL JOURNAL OF INNOVATIVE RESEARCH & DEVELOPMENT

ISSN: 2278 – 0211 (Online)

Underwater Explosion And Effect On Structures

S K Rao
Naval Architect Officer in the Indian Navy
M Tech in Ocean Engineering and Naval Architecture form IIT Kharagpur, India
Pursuing doctoral research in the field of underwater explosions and its effect on the structures
R Vijayakumar
Ph.D. from Indian Institute of Technology, Delhi, India
Adjunct Faculty at the Naval Construction Wing, Department of Applied Mechanics at Indian Institute of Technology, Delhi,India

Abstract:

The study of underwater explosions (UNDEX) on ship/submarines became of interest during World War II when torpedo explosions near a ship created more damage than a direct hit. Following the war, many full scale ship shock trials were conducted by various countries providing the empirical data that is widely employed. The biggest threat to any marine platform is due to underwater weapons and hence understanding the phenomenon is essential. The sequence of events involved in an UNDEX starting from the detonation, shock wave, bubble pulses and cavitation have been introduced and the dynamics of the process including governing laws have been enumerated in the paper. The associated aspects of loading and method of analyzing the fluid structure interaction have also been highlighted. The development of such numerical methods to analyze the explosion and its effect on the fluid-structure can lead to design of safer ships and submarines. Moreover, the numerical simulation will eliminate the need for conducting expensive shock tests and trials.

1.Introduction

The idea of using the explosive charges underwater to damage and sink the targets at sea has been there since the days of early Marine warfare, although the effective means to do it were limited or did not exist. This led to the need to understand the phenomenon, study the effects and in turn to design structures that can be protected from such high intensity dynamic loads.

In the pre WW-II era, almost all underwater explosive damage to naval ships was caused by contact explosions. At that time, one of the best ways to destroy a ship was to open a hole in the hull under the waterline by a direct hit and wait for flooding to reduce the stability of the ship so that the ship would sink. Aside from this, only a direct hit to a weapons magazine, an engine room or fuel tanks would result in the devastating loss of a ship. Since the result of a contact explosion is the destruction of the ship's structure in the immediate area of the explosion, only very slight effect of the explosion is transmitted to the other parts of the ship. In the late 1930s, the Bureau of Ships of US Navy performed experiments on small structural models of the naval vessels in the Norfolk Naval Shipyard in order to determine the underwater explosions (UNDEX) effects. Several tests were made in order to learn how to improve the strength of the hull to withstand the severe effects of underwater explosions. The tests led to understanding of the non-contact explosions that were found to cause severe underwater shock to the ships. When the non-contact underwater explosion occurred, the ship's back was broken as it was raised up and then struck down into the water. As a consequence, the ship sank into the gap left by the explosion. Increasing the charge weight resulted in more damage to the ship. Thus, it was understood that a direct hit was not necessary to disable the ship capabilities. According to the analysis of the wartime ship losses suffered during the first half of the twentieth century, it was determined that the incident shock wave and gas bubble pulse forces caused severe structural damage and material failure, and resulted in the sinking of several ships.

In spite of significant efforts by various agencies like government, military and civil resources directed towards mitigating the vulnerability of humans and structures due to the blast effects, it is widely accepted that the effects of the undex is still poorly understood. Moreover, the knowledge is not in public domain due to strategic reasons and hence not available to us. It is therefore of significance that theories and models capable of describing the phenomenon and its effects be developed to describe/understand the events qualitatively and quantitatively.

1.1.Undex Phenomenon

Underwater explosions, generally referred to as UNDEX, occurring in the water near the ship hull are of great concern to naval surface ships and submarines since they can result in major hull

Damage or incapacitate their functionality. Analyzing this phenomenon requires understanding a complex sequence of events, shock wave propagation, bulk cavitation and fluid-structure interaction phenomena. Underwater explosions may be classified in two categories 1.

- Contact underwater explosions: This type of explosion occurs in the water adjacent to or in contact with the hull of the ship, such as an impact-fused torpedo hit or the explosion of a contact mine. These explosions result in severe local damage to the hull.
- Non-contact underwater explosions: This type of explosion occurs at a given distance from the ship in water that is not in contact with the hull of the ship. The detonation of depth charges consisting of high explosives such as HBX-1, RDX, TNT and PETN is an example of non-contact underwater explosions. These explosions result in the most serious and severe shock damage to the ships.

1.1.1.Sequence Of Events

It is very important to understand the sequence of events that occurs in the water as a result of an underwater explosion. Any explosion (non-nuclear) is associated with a chemical reaction in a substance which converts the original material into gas at very high temperature and pressure in extreme rapidity. The temperatures and pressures involved are in the order of 3000^{o} C and 50,000 atm respectively. On detonation of a high explosive such as TNT, HBX-1, RDX, or PETN, a superheated, highly compressed gas bubble is formed along with a shock-wave in the surrounding water. The shock wave travels through the charge material at a constant high speed of approximately 25,000 ft/sec, without change in volume 2. This event happens very rapidly in order to prevent the energy from having enough time to escape. The high pressure gas compresses the surrounding water, that layer of water then compresses the adjacent layer, and so on. During these events, the compressibility of water is evident. As the gas expands, the water is forced radially outward and this radial flow modifies the pressure distribution at points relatively close to the bubble. Therefore, a shock front is propagated radially

outward at a velocity that exceeds the velocity of sound in the uncompressed water as shown in Figure 1.

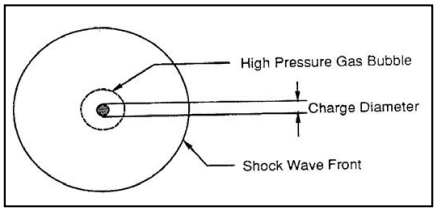

Figure 1: Gas Bubble and Shock Wave of UNDEX

1.1.2.The Shock Wave

A shock wave is characterized by a discontinuous change in pressure, particle velocity, and density in a direction normal to the front, followed by exponential decay in pressure down to the hydrostatic pressure. Figure 2 shows this type of pressure distribution for a 300 lb TNT underwater explosion 2.

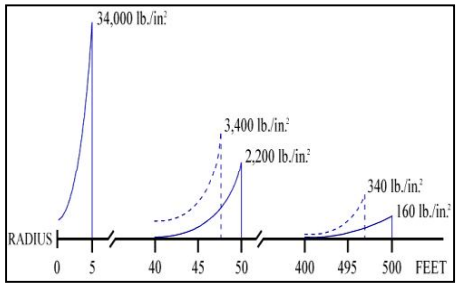

Figure 2: Shock Wave Pressure Profile for a Radially Expanding Wave from a 300lb TNT Charge

Initially the velocity of the shock wave is proportional to the peak pressure and hence several times of that of limiting acoustic value but with the wave advance and decay in pressures it falls to acoustic values (~1525 m/s). The pressure drop is due to the wave moving out in a spherical front. Thus, the resulting shock wave pressure profile is proportional to the charge weight and inverse of the distance from the charge.

1.1.3.Conditions At The Shock Front

In an explosive event excess pressures are created and hence the propagation of waves can no longer be considered constant rather they increase with increasing density. The density increases due to excess pressures. If we consider wave propagation in fluid, a

plane wave advancing from left to right and at an instant of time has a shape as shown in the figure 3.

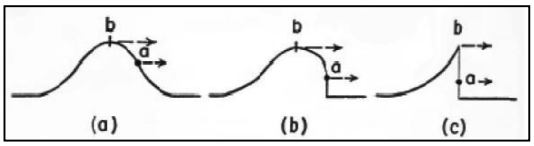

Figure 3: Formation of shock fronts in plane waves

Compression started in positive direction at point 'a' will appear to travel with a speed c_a relative to the fluid at that point. If the particle velocity excited in the fluid is 'u_a', the speed with respect to a fixed wall will be c_a+u_a. Similarly, a compression at point b will travel with a speed c_b+u_b. If the pressure set up in the fluid is greater at b than a, the speeds c_b & u_b will be greater and advance faster than those at 'a'. Therefore, the regions of higher pressure advance and to those of lower pressures and make the front increasingly steep. As the condition of infinite steepness is approached, the pressure and temperature of adjacent layers will be very different and hence large gradients. This leads to dissipation of energy as heat and hence the conventional equations of conservation of energy in the fluid will not be valid. However, experiments have shown that such fronts are so steep and virtually discontinuous. The equations applying to such discontinuity were originally developed by 'Rankine and Hugoniot' by considering the regions immediately ahead and behind the discontinuity (fig 4).

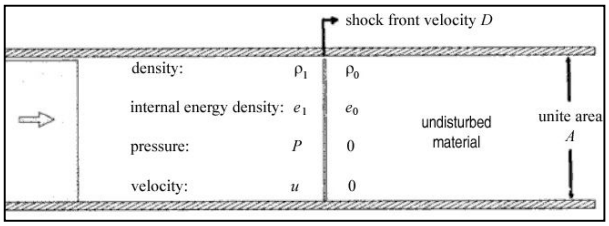

Figure 4: Conditions at a shock front moving with velocity 'D'.

Considering conservation of mass across the Shock front, $\rho_1(D-u) = \rho_0 D$;

Conservation of momentum yields, $\rho_0 Du\ dt = P\ dt$; i.e. the change in momentum must be equal to the impulse of pressure force in the limit $dt \to 0$. Hence, $\rho_0 Du = P$

Similarly conservation f energy yields, $Pu = \rho_0 D \left(e_1 - e_0 + \frac{1}{2} u^2\right)$

Eliminating P, we get, $e_1 = e_0 + \frac{1}{2} u^2$

The obtained equations are called as 'Rankine-Hugoniot' relations for the shock front.

1.1.4.Empirical Relations

Empirical equations are derived in order to characterize the shock wave pressure profile. These equations are accurate at distances between 10 and 100 charge radii and for duration of up to one decay constant in time after the initial detonation 2.

The pressure change with time follows an exponential decay and is given by the following equation for TNT explosive equivalents.

$$P = 52.4 \cdot (W^{1/3}/R)^{1.18}) \cdot (e^{(t-to)/\theta})$$

where, W is the weight of the TNT explosive in kg,

t_0 is the initial time at which the shock front arrives at a distance R in meters,

t is the times elapsed since the shock wave has arrived at that distance and

$\theta = 0.084 \cdot W^{1/3^*} \cdot (W^{1/3}/R)^{-0.23}$, is the decay constant or the decay time in seconds, the time taken for the pressure to decay to 1/e, translating roughly to 36.79% of the peak pressure.

1.1.5.The After Flow

As the shock wave passes a fixed location and subjects the water to a transient pressure, the liquid is simultaneously subjected to a flow with a velocity in the direction of the wave. The velocity of the water (plane waves) is related to the transient pressure by

$u(t) = P(t)/\rho c$, P(t) being the transient pressure, ρ is the density of water and c is the sound speed in water.

The work done on a surface or the shock wave flux density i.e the energy behind the shock front per unit area assuming planar wave front is given by,

Energy flux density = $\int_0^t P(t)\, u(t) dt = \frac{1}{\rho c} \int_0^t P^2(t)\, dt$

If the spherical wave front is taken, the amplitude of the shock wave decreases inversely with the distance from the detonation point as the disturbance spreads to greater area. In most applications, planar shock wave theory is sufficient.

1.1.6.The Gas Bubble

The gas bubble generated by the explosion is almost spherical in its initial stages and starts expanding as the inside pressure is significantly higher than the ambient hydrostatic pressure. After some time, the expanding gas bubble pressure drops to the hydrostatic pressure. But the adjacent water still has an outward velocity and hence the gas bubble does not rest and continues to expand until the pressure defect prevents further expansion. At this instant, the gas bubble reaches its maximum radius and the internal energy of the gas bubble is so small that it can be neglected. The maximum bubble radius depends on the charge type, depth and weight and is given by (for TNT)

$$R_{max} = 3.50 \cdot (W^{1/3} / Z_0)^{1/3}$$

Where Z_0 is the total pressure head at the explosive i.e $Z_0 = D + 9.8$, D being the explosion depth in meters. The time taken to reach the maximum diameter is given by

$$T = 2.11 \cdot (W^{1/3} / Z_0^{5/6})$$

After reaching the maximum radius, the gas bubble pressure becomes so small that the excess hydrostatic pressure causes the gas sphere to be contracted to ambient and then due to inertial effects, recompressed to a high pressure determined by the inward velocity of the water at the equilibrium pressure. Due to this recompression, a second wave forms and radiates into the water. The second bubble again reaches its equilibrium state and a maximum radius which is smaller than initial maximum radius. The gas sphere can undergo several compressions and re-expansions until it loses all of its energy or the bubble reaches a boundary. Figure 5 shows the asymmetric oscillations of the bubble about its mean diameter.

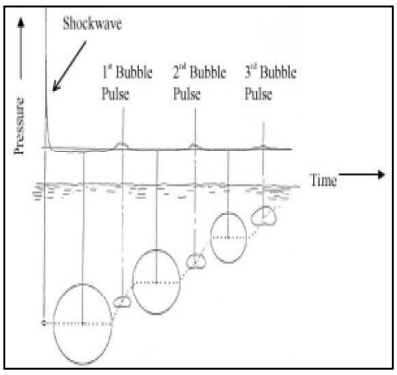

Figure 5: Migration Pathway and Gas Bubble Oscillation 4

The peak pressure of the bubble at its first minimum size is approximately 10-15% of the shock wave peak pressure. It can be further reduced due to migrations towards surface. The bubble pressure pulses can also result in localized damage to hull structures. Moreover, the large bubbles often lose their symmetry and collapse upon themselves forming a toroid shaped bubble and jet of water. This combination of bubble pulse and water jet can produce significant damage.

As the gas bubble expands it displaces water surrounding it. During the contraction, the water rushes in to surround the volume vacated by the bubble. The vertical bubble velocity can be shown to be inversely proportional to the cube of the bubble radius and hence the bubble rises faster when its size is minimum. Though the buoyancy is maximum when the bubble is large, the inertial forces of the surrounding water dominate and hence cancel out the buoyancy to a large extent. The inertial forces are lowest at its extreme size and the buoyancy pushes it at maximum rate 2.

Depending on the initial depth of explosion, the bubble may migrate close to surface during its oscillations. If the bubble gets close to the surface, it results in the characteristic plumes of water that occur just after the surface cavitation due to shock wave. The expansion of the bubble displaces water radially creates a matching plume. If the first bubble expansion does not break through the water surface, the first plume appears broad and low. Consequent oscillations migrate the bubble closer to the surface and may breach the surface during the second or third maximums, as after these the energy dissipates dramatically. On breach of surface, the plume is thinner and higher and may be blackened due to venting of the explosion gases containing carbon rich products.

In shallow water, the pressure in the expanding gas bubble can fall below the atmospheric pressure leading to air entering the cavity very rapidly when the gas bubble reaches the surface. This acts as a cushion and allows the closure, eliminating any closure pressure pulse. Therefore, it can be stated that the explosion depth should be less than the maximum bubble radius. However, the results will be acceptable if the charge depth is between 50% and 80% of maximum radius 6.

As it can be seen that the depth has strong influence on the underwater explosions, they can be categorized in accordance with their depth beneath the water's surface and energy associated with it. An underwater explosion can be considered as shallow if $(d/W^{1/3}) < 1$ and deep if the ratio is greater than 16. (Here the d is depth in feet and W is pounds of TNT[7]).

1.1.7.Empirical Equations

The equations discussed can be generalized and can be applied for different explosives as give below:

Pressure = $(K1 . (W^{1/3}/R)^{A1})* e^{(t-to)/\theta}$ (MPa)
Peak Pressure = $K1. (W^{1/3}/R)^{A1}$ (MPa)
Decay Constant = $K2. W^{1/3}.(Wl/3/R)^{A2}$ (ms)
Impulse = $K3. W^{1/3}. (W^{1/3}/R)^{A3}$ (MPa-see)
Energy Flux Density = $K4. W^{1/3}. (W^{1/3}/R)^{A4}$ (m-kPa)
Bubble Period = $K5. W^{1/3}/(D+9.8)^{5/6}$) (see)
Bubble Radius = $K6. W^{1/3}/(D+9.8)^{1/3}$) (m)

Where, W stands for charge weight in kg, R are the slant stand-off distance in meters and D is the charge depth in meters. The constants used in the equations are as given in the table 1 for different explosives.

Table 1 : Coefficients for shock definition

:	Coefficient	HBX-1 ref (3)	TNT ref (3)	PENT ref (3)	NUCLEAR ref (7)
Shock-wave	K1	53.51	52.12	56.21	1.06E4
Pressure	A1	1.144	1.18	1.194	1.13
Decay	K2	0.092	0.092	0.086	3.627
Constant	A2	-0.247	-0.185	-0.257	-0.22
Impulse	K3	7.263	6.52	6.518	4.5E4
	A3	0.856	0.98	0.903	0.91
Energy Flux	K4	106.8	94.34	103.11	1.15E7
Density	A4	2.039	2.155	2.094	2.04
Bubble	K5	2.302	2.064	2.098	249.1
Period					
Bubble	K6	3.775	3.383	3.439	400.5
Radius					

Table 1:Coefficients for shock definition

1.1.8.Energy Contents

The majority of the energy associated with Undex is released in the form of shock wave accounting for approximately 53%, leaving the rest for gas bubble pulsations. Of the shock wave energy, 20 % is lost during early propagation i.e with in 25 times the charge radii of explosion and only 33% will be available as damaging energy. During the bubble pulsation, 13% of the explosion energy is radiated during the first cycle, 17% is radiated as a pressure pulse at bubble first minimum. The balance 17% of the explosion energy is available for the second pulsation.

The proximity of boundary affects the behavior of explosions. When the shock wave reaches the surface it usually produces a visible spray dome due to surface cavitation. Reflection of shock wave off ocean floor can augment the effect of the initial shock. In

shallow waters, reflection factors of 1.4 can be accomplished that can dramatically increase the damage potential.

1.2.Principle Of Similarity Of Shock Wave

The principle of similarity states that if the linear size of the charge be changed by a factor *k*, the pressure conditions will be unchanged, if new distance and time scales *k* times as large as the original ones are used 2.

The principle is very evident from the empirical relations shown earlier and is an outcome of the similarity that is valid in governing equations of state. It has been amply verified by experimentation. The principle is valid as long as there are no external forces acting upon the system. Though gravity is such an external force which is always present, it is insignificant compared with the internal forces involved in generation and propagation of shock waves. However, gravity plays a significant role in behavior of gas bubble pulsations and hence the similarity does not apply to the post shock wave phenomena.

1.3.Cavitation

The reflection of the shock wave from the free surface of water leads to the phenomenon called 'Cavitation'. A tensile reflected wave, which is called rarefaction wave, occurs when the compressive shock wave is reflected from the free surface. Water cannot support the tensile force and hence the cavitation when the pressure falls to vapor pressure of water. There are two types of cavitation in an UNDEX event: bulk cavitation and local cavitation. Bulk cavitation can be regarded as the large area of low pressure at the free surface whereas local cavitation can be regarded as the small area of low pressure occurring at the fluid-structure interface. Cavitation has a tremendous effect on the overall response of the surface ships so that it must be taken into consideration in the damage simulations 4.

1.3.1.Bulk Cavitation

In an underwater explosion, a three-dimensional spherical pressure wave forms and propagates outward from the detonation center. As shown in Fig 6, the incident shock wave, which is compressive reaches the free surface and is reflected. The reflection phenomena can be approximated to that of the acoustic as long as the pressure involved are less than 68.95 MPa and incident angles are less than 30^{o}. Accordingly, the reflected

shock wave is a rarefaction wave and the direction is opposite to that of the incident. Since the air-water interface is not a rigid boundary, the surface of water will be thrown up at twice the velocity of that of the normal component of incident velocity. The rarefaction wave is like a tensile wave and reduces the pressure as it progresses. It like a tensile wave produced by an image source across the surface. As the water cannot support the tensile force, it forms cavities with water vapor. After the arrival of the rarefaction wave, the net pressure drops to zero or negative value as shown in the figure 7. This is called "cut-off" in the pressure. The cavitation pressure is a negative pressure of three to four psi 9. A bottom reflection wave is also formed due to the reflection of the shock wave at the sea bottom. However, this type of wave is of less interest in an UNDEX event due to the dependence on the sea bottom characteristics and its closeness to the target.

The cavitated region formed by the rarefaction wave is called the bulk cavitation zone. It consists of two boundaries: the upper cavitation boundary and the lower cavitation boundary. The upper cavitation boundary is the region where the net pressure due to incident and reflected waves is zero. In fact, the net pressure below the surface is not zero at the cut-off time. The calculated net pressure may be less than zero depending on the depth.

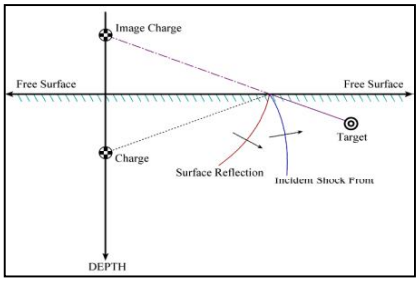

Figure 6: Reflection of Shock wave from Free Surface

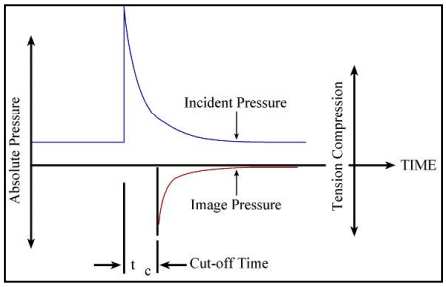

Figure 7: Shock Wave Pressure Profile with Cut-off [10]

As stated before, cavitation occurs where the total pressure is negative or below the vapour pressure. Total pressure consists of compressive incident wave pressure, tensile rarefaction wave pressure, atmospheric pressure and hydrostatic pressure. The following equation can be used to determine the upper cavitation boundary.

The total pressure = $$K_1\left(\frac{W^{\frac{1}{3}}}{r_1}\right)^{A_1} e^{\frac{-(r_2-r_1)}{C\theta}} + P_A + \gamma y - K_1\left(\frac{W^{\frac{1}{3}}}{r_2}\right)^{A_1} = 0$$

Here, the r_1 and r_2 are the slant stand-off distances to the point from the charge and image charge respectively. C is the acoustic velocity, P_A is the atmospheric pressure, γ is the weight density of water and W is the charge weight. The constants are as shown in the table 1.

The lower cavitation boundary is determined by equating the decay rate of breaking pressure and the decay rate of absolute pressure. The breaking pressure is defined as the rarefaction wave pressure that reduces the absolute pressure to the cavitation pressure. The following equation can be used to determine the lower cavitation boundary.

i.e

$$-\frac{P_i}{C\theta}\left\{1+\left[\frac{r_2-2D\left(\frac{D+y}{r_2}\right)}{r_1}\right]\left[\frac{A_2 r_2}{r_1}-A_2-1\right]\right\}$$

$$-\frac{A_1 P_i}{r_1^2}\left[r_2-2D\left(\frac{D+y}{r_2}\right)\right]+\gamma\left(\frac{D+y}{r_2}\right)+\frac{A_1}{r_2}(P_i+P_A+\gamma y)=0$$

Here, P_i is the incident shock wave pressure and others are as discussed earlier.

The above equations can easily be modeled using tools like MATLAB and typical cavitation boundary can be obtained. Fig 8 shows such boundaries for different charge weights and charge depths.

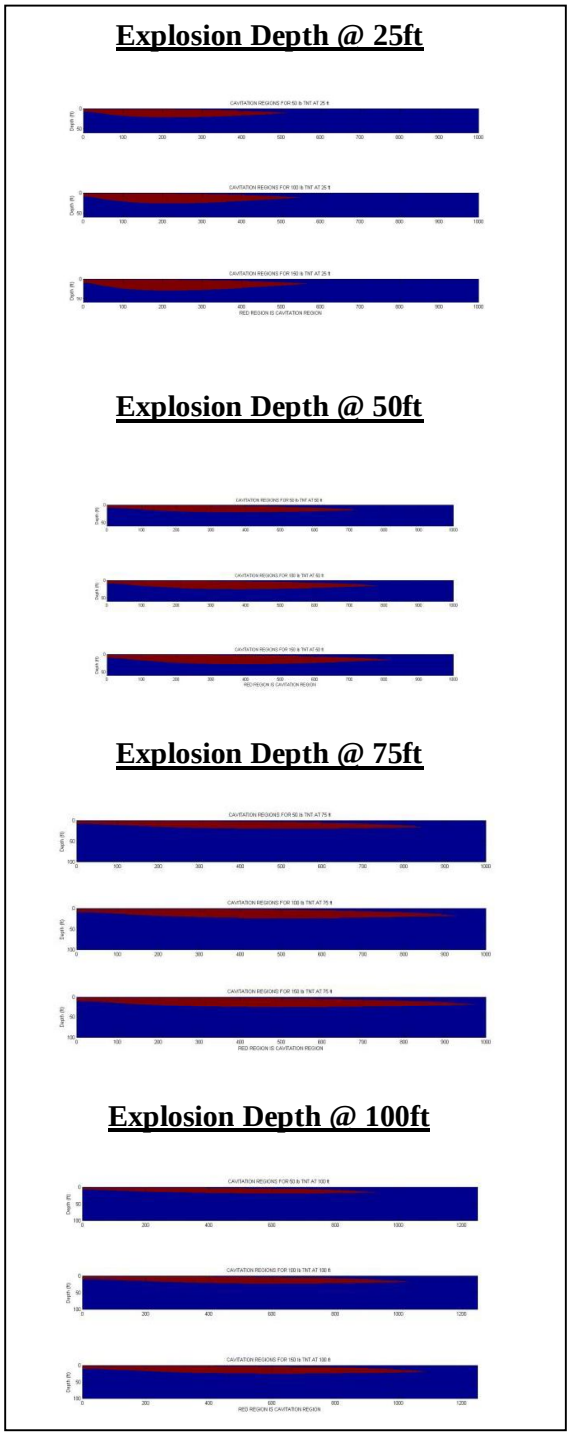

Figure 8: Cavitaion regimes for differing weight and explosion depth for TNT

It is evident from the above figures that the cavitation boundaries are highly dependent on the charge type, weight and depth as seen in the earlier equations. The plots are generated for 50lbs-150lbs Trinitrotoluene (TNT) charge at varying depths i.e. 25 ft-100 ft. As shown in Figure 6, the cavitation region (shown in red) stretches as the charge

depth increases and the vertical depth of the region decreases due to the stretching. Therefore, the cavitation area is the largest when the charge is deeper. Also, the cavitation area increases with increasing charge weight. The cavitation area also is affected by the type of explosive. The cavitation phenomenon has significant effect on the structure adjacent to it and hence damage can be maximized by suitable combination of explosive type, weight and depth.

If the explosion considered is below a floating ship, the vertical kick-off velocity of the surface ship can be determined by the fluid particle velocities near the free surface. Moreover, due to fluid-structure interaction at the hull surface causes another phenomenon called "Local cavitation"10.

1.3.2.Local Cavitation

Local cavitation is the phenomenon that occurs at the fluid-structure interface due to the interaction of the pressure pulse and the flexible surface of the structure. The shock pressure pulses that are produced by an UNDEX event excite the ship causing dynamic responses leading to negative total pressure along the hull. As water cannot support tensile pressure, the water pressure drops to the vapor pressure of water and local cavitation occurs.

1.4.Fluid-Structure Interaction

Taylor flat plate theory, which was presented by G. I. Taylor, is the simplest fluid-structure interaction theory. Here, an infinite, air-backed plate is used as the hull in order to illustrate the reaction of the hull subjected to the shock wave, as shown in Figure 9.

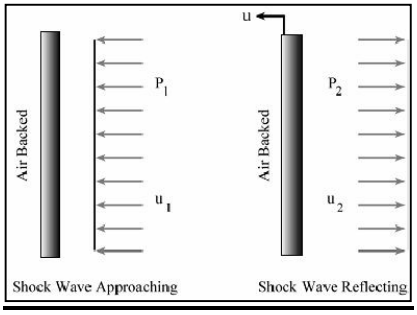

Figure 9: Taylor Plate Subjected to a Plane Wave

As shown in the figure, the plate is subjected to the incident plane shock wave of pressure, $P_1(t)$. After interacting with the plate, the reflected plane shock wave of pressure is of pressure say $P_2(t)$. According to Newton's 2nd Law, the equation of motion of the plate can be written as

$$m\frac{du(t)}{dt} = P_1(t) + P_2(t)$$

Where, m = the mass of the plate per unit area and $u(t)$ = the velocity of the plate.

The velocities of the fluid particle behind the incident and reflected shock waves are defined as $u_1(t)$and $u_2(t)$, respectively. Thus, the velocity of the plate can be defined as

$$u(t) = u_1(t) - u_2(t)$$

For planar shock waves, the wave pressures can be expressed as

$$P_1(t) = \rho C u_1(t) \text{ and } P_2(t) = \rho C u_2(t),$$

Where, ρ = the fluid density, C = the acoustic velocity.

Hence, the plate velocity can be related to the shock wave pressure as,

$$u(t) = u_1(t) - u_2(t) = \frac{P_1(t) - P_2(t)}{\rho C}$$

Hence, $P_2(t)$ is give by

$$P_2(t) = P_{\max} e^{-\left(\frac{t-t_1}{\theta}\right)} - \rho C u(t)$$

Using the above and substituting the formulae for the shock wave pressure in to the equation of motion of plate,

$$m\left(\frac{du}{dt}\right) + \rho C u(t) = 2P_{\max} e^{-\left(\frac{t-t_1}{\theta}\right)}$$

This is a first order linear differential equation and can be solved for u(t) and is given by the below expression.

$$u(t) = \frac{2P_{\max}\theta}{m(1-\beta)}\left\{e^{-\left[\frac{\beta(t-t_1)}{\theta}\right]} - e^{-\left[\frac{(t-t_1)}{\theta}\right]}\right\}$$

where, $\beta = \rho C\theta/m$ and $t>0$. Using the equation of plate velocity, the pressures can be calculated as give below.

$$P_2(t) = \frac{P_{\max}}{1-\beta}\left[(1+\beta)e^{-\left(\frac{t-t_1}{\theta}\right)} - 2\beta e^{-\left[\frac{\beta(t-t_1)}{\theta}\right]}\right]$$

$$P_1 + P_2 = P_{\max}\left\{\frac{2}{1-\beta}e^{-\left[\frac{(t-t_1)}{\theta}\right]} - \frac{2\beta}{1-\beta}e^{-\left[\frac{\beta(t-t_1)}{\theta}\right]}\right\}$$

From the above equations, it is evident that the total pressure becomes negative initially as β increases i.e valid for a light plate in water. The negative pressure leads to cavitation of the water and hence separation of plate from water. The maximum velocity of the plate will be when it is subjected to the shock front and that instance the total pressure of the incident and reflected shall be zero. The same can be verified by differentiating the equation of u(t) with respect to time and substituting the value of β in the above equation.

the cut-off time is $t_0 = \frac{\ln \beta}{\beta - 1}\theta$ given by,

The maximum velocity of the plate,

$$u_{\max} = \frac{2P_{\max}\theta}{m(1-\beta)}\left[e^{-\left(\frac{\beta t_0}{\theta}\right)} - e^{-\left(\frac{t_0}{\theta}\right)}\right]$$

It is to be noted that the equations used in the Taylor plate theory are appropriate up to the beginning of the cavitation. Post cavitation, the problem turns into a nonlinear and non-conservative and the above equations are no longer valid. For light plates, the momentum of the plate can be a fraction of the impulse of the shock wave and hence can lead to further increase in velocity and second loading which can be higher than the first loading 11.

1.5.Shock Factor

The accurate theoretical evaluation of the undex phenomenon is quite complex and hence model testing and numerical experiments using simplifying assumptions are often used. However, it is important to correlate such results to that of real structure to an acceptable accuracy.

The most widely used parameter to describe the shock severity and hence its damaging potential is "Shock Factor" (SF). It is also called as "Hull shock factor" when applied to ships. Higher the SF, higher is the energy content impinged on the structure. Hence, the response and excited damage can be estimated in terms of the SF [11]. It has been found that,

SF = W^n/D, W is the charge weight and D is the stand-off distance. The value of "n" varied for different experimental conditions and the method followed. One of the most used value of n is 0.5. When the charge position is measured to relative to the ship's

keel, the angle of incidence of shock-wave should be considered and such calculated SF is often called "Keel Shock factor (KSF)". It is give as 18,

$$SF = \frac{(1+\cos\theta)}{2}\frac{\sqrt{W}}{R}$$

Here, θ is the angle between the vertical line through the charge and the line drawn through the charge to the ship's keel. It can be seen that if charge is directly underneath the keel, $\theta=0^o$ and hence KSF = SF. It has been shown through theory and experimentation that the KSF is approximately proportional to the vertical velocity imparted to the ship when it behaves like a rigid body.

Use of shock factors eliminates the need for elaborate analysis and is the simplest way to compare or know the severity of an explosion and the likely extent of structural damage. However, experimental or validated numerical investigation is necessary to establish the propagation of shock through the body and the accelerations/ velocities induced in the body.

2.Numerical Solution And Modeling

Explosion loading on structures is essentially a transient analysis involving time variance in the loading pattern. The explosion event is an instantaneous process with characteristic exponential amplitude decay with time, this aspect demands on using smaller time steps and explicit schemes for a stable convergent analysis. The explosion loading related problems are best solved by numerical discretisation techniques such as the finite element method. Today, large spectrums of finite element codes are available which can perform explosive loading analysis to certain degree of accuracy involving certain assumptions. The problem in hand is further very stringent in terms to say, it involves material and geometric nonlinearity with strain rate dependence, these important factors are seen to have a great effect on the congruence of results with experiments. The present analysis involves solving the nonlinear equations using finite elements (discrete model) on a digital computer. The numerical model is essentially elasto-plastic in nature incorporating stress-strain relationships to define material plasticity (with strain rate dependence) and also material failure. The material plasticity and strain rate dependence are modeled using Johnson-Cook relationships. The numerical model is further described in the following paragraphs in terms of some salient features as used in the present study.

The basic steps involved in a numerical simulation are;

- Mathematical modeling or idealization - This step involves in formulating the desired physical phenomenon into a mathematical solvable form in terms of equations representing the system to best describe the physical problem considering the accuracy desired.
- Discretization - This is the basic step in any finite element approach of solution to the defined mathematical problem. The step involves breaking up of the physical domain into smaller solvable entities by numerical iterative methods with finite degrees of freedom.
- Solution on a digital computer - The numerical scheme so formed after discretization is solved using a digital computer.
- Post processing of results - The interpretation of the numerical results in terms of their mathematical and physical significance. The result post processing is the key to correctness of the results when it comes to nonlinear analysis. The importance of the same has been brought out in selection of the correct constitutive relationship in the present study.

4.1.Sources Of Non-Linearity

One needs to explore and study the source of nonlinearity is required to simulate such physical behavior with mathematical and computational models. For structural analysis there are four sources of nonlinear behavior. The corresponding nonlinear effects are identified by the terms material, geometric, force boundary condition and displacement boundary condition (BC) that need to be sufficiently modeled for acceptable results.

4.2.Johnson-Cook Constitutive Relationship

JC material model is employed for analyzing the behavior of the structure under dynamic loading to account for increasing yield strength due to hardening. The rate dependence is also employed. This plasticity model incorporates a distortion energy theory using the von Mises yield criteria with associated flow rule. The hardening in the JC model is of isotropic hardening type where the static yield stress, σ_o, is given by;

$$\sigma^{O}=[A+B(\dot{\varepsilon}^{pl})^{n}](1-\bar{\theta}^{m}),$$

where, $\dot{\varepsilon}^{pl}$ is the equivalent plastic strain, $\theta_{transition}$ is the transition temperature, $\bar{\theta}$ is the non-dimentional temperature,

the limits of $\bar{\theta}$ is defined as;

$\bar{\theta} = 0 \text{ for } \theta < \theta_{transition}$

$\bar{\theta} \equiv \left\{ \frac{\theta - \theta_{transition}}{\theta_{melt} - \theta_{transition}} \right\} \text{ for } \theta_{transition} \leq \theta \leq \theta_{melt}$

$\bar{\theta} = 1 \text{ for } \theta > \theta_{melt}$

where θ is the current temperature, θ_{melt} is the melting temperature, and $\theta_{transition}$ is the transition temperature defined as the one at or below which there is no temperature dependence on the expression of the yield stress.

A, *B*, *n* and *m* are material parameters measured at or below the transition temperature.

$$\bar{\sigma} = \sigma^{\circ}(\bar{\varepsilon}^{pl}, \theta) R(\dot{\bar{\varepsilon}}^{pl})$$

The Johnson-Cook strain rate dependence formulation is in the form;

and $\dot{\bar{\varepsilon}}^{pl} = \dot{\varepsilon}_0 \exp[\frac{1}{C}(R-1)]$, where

$\bar{\sigma}$ is the yield stress at non-zero strain rate; $\dot{\varepsilon}_0$and *C* are material parameters measured at or below the transition temperature;$\sigma^0(\overline{\varepsilon^{pl}}, \theta)$ is the static yield stress; and $R(\bar{\varepsilon}^{pl})$is the ratio of the yield stress at nonzero strain rate to the static yield stress

The yield stress is, therefore, expressed as

$$\bar{\sigma} = [A + B(\bar{\varepsilon}^{pl})^n]\left[1 + C \ln\left(\frac{\bar{\varepsilon}^{pl}}{\dot{\varepsilon}_0}\right)\right](1 - \hat{\theta}^m)$$

4.3.Johnson-Cook Dynamic Failure

The Johnson-Cook plasticity model is suitable for high-strain-rate deformation of metals. The Johnson-Cook dynamic failure model is based on the value of the equivalent plastic strain at element integration points; failure is assumed to occur when the damage parameter exceeds unity. The damage parameter, ω, is defined as

$$\omega = \sum\left(\frac{\Delta\bar{\varepsilon}^{pl}}{\bar{\varepsilon}_f^{pl}}\right)$$

Where $\Delta\bar{\varepsilon}^{pl}$ is an increment of the equivalent plastic strain, $\bar{\varepsilon}^{pl}{}_f$is the strain at failure, and the summation is performed over all increments in the analysis. The strain at failure, $\bar{\varepsilon}^{pl}{}_f$, is assumed to be dependent on a non-dimensional plastic strain rate, $\frac{\bar{\varepsilon}^{pl}}{\dot{\varepsilon}_0}$; a dimensionless pressure-deviatoric stress ratio, p/q (where *p* is the pressure stress and *q* is

the Mises stress); and the non-dimensional temperature, $\hat{\theta}$, defined earlier in the Johnson-Cook hardening model. The dependencies are assumed to be separable and are of the form,

$$\bar{\varepsilon}^{pl}{}_f = \left[d_1 + d_2 \exp\left(d_3 \frac{p}{q}\right)\right]\left[1 + d_4 In\left(\frac{\bar{\varepsilon}^{pl}}{\varepsilon_0}\right)\right](1 + d_5\hat{\theta}),$$

where d_1–d_5 are failure parameters measured at or below the transition temperature, $\theta_{transition}$, and $\dot{\varepsilon}_0$is the reference strain rate. When this failure criterion is met, the deviatoric stress components are set to zero and remain zero for the rest of the analysis. The pressure stress in turn can be set to zero for the rest of calculation and one may specify element deletion which meet the failure criterion.

4.4.Explicit Dynamic Analysis Method

A transient dynamic analysis with strain update was adopted in the present analysis. The strain update and plasticity has been brought about by the JC constitutive relationship for plasticity and failure, the status of the elements in the event of material failure has been brought about by the JC dynamic failure with progressive damage initiation and degradation formulation. Due to the rapidly changing nature of the loading in the UNDEX loading a transient analysis has been chosen for solution.

A general linear transient dynamic equilibrium equation can be defined as;

$$[M]\{\ddot{u}\} + [C]\{\dot{u}\} + [K]\{u\} = \{F^{ex}\}$$

Where,

[M], [C]& [K] are the structural mass damping and stiffness matrices respectively,

$\{\ddot{u}\}$, $\dot{u}$, {u} are theacceleration, velocity and displacement vectors respectively, at integration point

$\{F^{ex}\}$ is the applied explosive load vector including fluid effects.

4.5.Fluid Structure Interaction (Fsi) Using Doubly Asymptotic Approximation

The fluid-structure interaction between the water and the hull due to the underwater explosion mainly occurs in the vertical direction. Since the shock wave impinges on the ship hull causing dynamic responses on the ship structure, the fluid-structure interaction has a great importance in an UNDEX event. A matrix of differential equations is used to determine the approximate response of the ship with some acceptable degree of accuracy. This approximation is called the Doubly Asymptotic Approximation (DAA)

and is applicable at both low and high frequencies and at early and late times. The DAA approach models the acoustic medium surrounding the structure as a membrane covering the wet surface of the structure. The principal advantage is that it eliminates the need for analyzing fluid volume elements around the outside of the structure. The DAA may be used to determine the fluid pressure generated by the scattered wave on the wet surface of the structure[3]. The governing equation of motion for the structure and the DAA equation with the interface compatibility relation are used to solve the dynamic response of the system. The discretized differential equation for the structure can be expressed as

$$M_s\ddot{x}(t) + C_s\dot{x}(t) + K_s x(t) = f(t)$$

Where, x(t) is the structural displacement vector, M_s, C_s and K_s are mass, damping and stiffness matrices, respectively, f(t) is the external force vector and a dot denotes a time derivative. For excitation of a submerged structure by an acoustic wave, f(t) is given by

$$f(t) = -GA_f[p_i(t) + p_s(t)] + f_d(t)$$

where $p_i(t)$ and $p_s(t)$ are nodal incident(known) and scattered(unknown) wave pressure vectors for the wet-surface fluid mesh, respectively, $f_d(t)$ is the applied force vector for the dry-structure, A_f is the diagonal area matrix converting nodal pressures to nodal forces and G is the transformation matrix associated with fluid and structural nodal surface forces.

The first-order doubly asymptotic approximation can be expressed as

$$M_f\dot{p}_s(t) + \rho c A_f p_s(t) = \rho c M_f \dot{u}_s(t)$$

Where, M_f is the fluid mass matrix for the wet-surface fluid mesh, ρ and c are the density and acoustic velocity of the fluid, respectively, and $u_s(t)$ is the vector of scattered wave fluid particle velocities normal to the structure wet surface. The name "doubly asymptotic" is because the equation exhibits the correct asymptotic behavior in both the high-frequency (early time) and low-frequency (late-time) limits. For high-frequency motion, the acceleration term is significantly higher than $p_s(t)$, so that the second term in the left-hand side of equation is negligible compared with the first term resulting in the plane wave approximation,

$$p_s(t) = \rho c u_s(t)$$

which is accurate for sufficiently short acoustic wavelengths. For low-frequency motion, $p_s(t)$ term is significantly higher and hence the DAA equation approaches the virtual mass approximation $A_f\, p_s\,(t) = M_f u_s(t)$ which is accurate for sufficiently long acoustic wavelengths.

The fluid–structure interface compatibility relation can be expressed as

$$G^{\mathrm{T}}\dot{x} = u_{\mathrm{i}} + u_{\mathrm{s}}$$

where the superscript 'T' denotes matrix transposition. The equation (xx) expresses the fluid particle velocity and the structural velocity normal to the set-surface of the structure are equal at the interface.

From manipulations of the above equations and assuming $f_d(t)$ is zero, we get,

$$M_{\mathrm{s}}\ddot{x} + C_{\mathrm{s}}\dot{x} + K_{\mathrm{s}}x = -GA_{\mathrm{f}}[p_{\mathrm{i}}(t) + p_{\mathrm{s}}(t)]$$

$$M_{\mathrm{f}}\ddot{p}_{\mathrm{s}}(t) + \rho cA_{\mathrm{f}}p_{\mathrm{s}}(t) = \rho cM_{\mathrm{f}}[G^{\mathrm{T}}\ddot{x}(t) - \dot{u}_{\mathrm{i}}]$$

The above equations can be solved simultaneously at each time step for x and p_s. The DAA approach is excellent approximation technique to eliminate the need for modeling surrounding fluid volume, and covering the wet surface of the structure with DAA boundary elements. Such a methodology is implemented by various FE codes for solving the undex related fluid-structure interaction.

5.FE Model & Discussion Of Results

The numerical finite element modeling was carried out to study the effect of the underwater explosion loads on a rectangular flat plate of 4 mm thickness including the fluid-structure interaction. The results were compared with that of the published experiments[10&11] for validation. The mesh size and the material model were evolved to obtain the results to the desired accuracy. Quarter size plate can be considered to reduce the computational time required. The four node Shell elements with reduced integration, S4R were used in the Abaqus Explicit model.

The model was prepared in Abaqus. The loading was established using the UNDEX module. The material model used for defining the plasticity of the model was that given by Johnson and Cook. To improve the results to sufficient accuracy, the effect of J-C strain hardening and rate dependency were considered in the model. Fig 10 shows that the central deformations agree well with the experiment, validating the FE model. The loading was varied in terms of the undex shock factor (generally keeping a constant stand-off distance and increasing the charge mass).

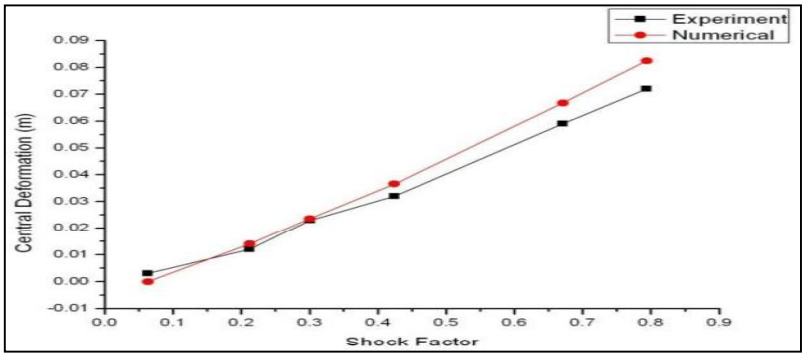

Figure 10: Comparision of Central Deformation

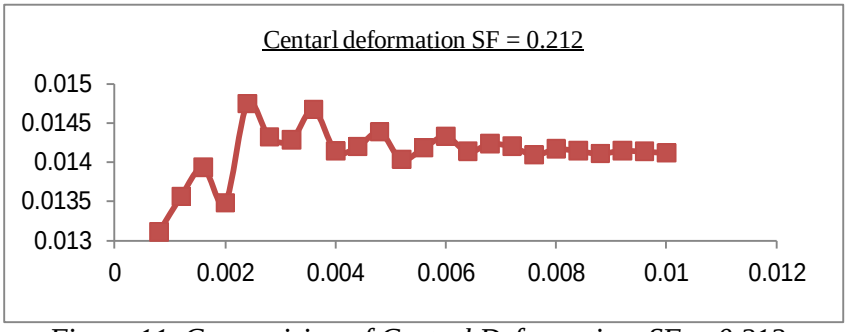

Figure 11. Comparision of Central Deformation, SF = 0.212

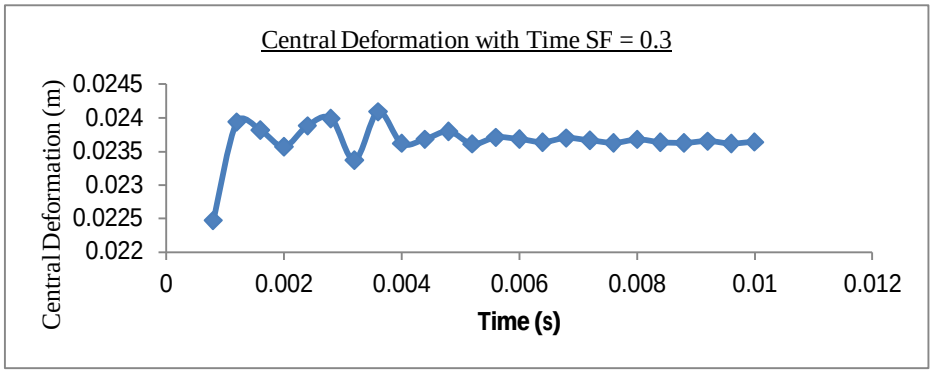

Figure 12: Plot of Central Deformation with time, SF = 0.3

The plots of the central deformation are shown in Fig 11 for two different shock factors. The plots show the central deformation of the plate as a function of time at different instants of time. The plate actually vibrates when subjected to an UNDEX load and the same is visible from the following graphs.

In all the graphs, it can be seen that analysis of a time period of 10 ms was sufficient for the adopted stand-off distance of 0.15 m from the centre of the plate. The maximum deformation of the plate at all the considered loading was seen to be at 4 ms, beyond which the response decayed considerably leaving the permanent deformation.

6.Conclusion

The Finite element model of a flat plate subjected to underwater blast was considered. The large deformations associated with the phenomenon were modeled using 3D non-linear FEM, including the effect of strain hardening and rate dependency of the strength. A quarter plate was modeled with symmetric boundary conditions with optimized mesh density. All the loading considered under the considered shock factors was limited to Mode I behavior of the plate, the undergoing large deformations.

The loading due to underwater explosion is different from any impact/ impulse that is effective for a short duration of time. The undex loading is characteristic with its exponential decay and the dense water medium has a significant effect on the behavior of the structure.

7.Reference

1. NAVSHIPS 250-660-26, "Mechanical Shock on Naval Vessels," March 1946.
2. Cole, R. H., Underwater Explosions, Princeton University Press, 1948
3. M.R. Driels,1980, "The effect of a non-zero cavitation tension on the damage sustained by a target plate subject to an underwater explosion.", Journal of Sound and Vibration.
4. Ucar, H. "Dynamic response of catamaran hull ship subjected to underwater explosions." Naval Postgraduate School, Monterey, California,2006.
5. Geers, T. L." Doubly Asymptotic Approximations for Transient Motions of Submerged Structures". J. Acoust. Soc. Am., Vol. 64, 1978, p. 1500-1508.
6. Y.S. Shin, D.T. Hooker, "Damage response of submerged imperfect cylindrical structures to underwater explosion", Computers and Structures, Vol. 60, Pp.683-693 , 1996.
7. Le Méhauté, B., Wang, S. "Water waves generated by underwater explosion."
8. World Scientific Publishing. ISBN 981-02-2083-9. (1995).
9. Klaseboer, E., Hung, K.C., Wang, C., Wang et al." Experimental and numerical investigation of the dynamics of an underwater explosion bubble near a resilient/rigid structure. J. Fluid Mech. 537:387–413.(2005)
10. R. Rajendran, K. Narasimhan, "Linear elastic shock response of plates subjected to underwater explosion", International Journal of Impact Engineering, Vol. 25, Pp.493-506 , 2001.
11. K. Ramajeyathilagam, C.P Vendhan, V.B. Rao, "Non-linear transient dynamic response of rectangular plates under shock loading", International Journal of Impact Engineering, Vol. 24, Pp.999-1015 , 2000
12. Bangash, M.Y.H. Shock, Impact and Explosion:Structural Analysis and Design. Springer, 2009
13. JamesL. O'Daniel , Theodor Krauthammerb, Kevin L. Koudelab,Larry H. Straitb, "An UNDEX response validation methodology",US Army Engineer Research and Development Center, Structural Mechanics Branch, International Journal of Impact Engineering 27 (2002), 919-937.
14. Liviu Librescu, Sang-Yong Oh and Joerg Hohe, "Implication of Nonclassical Effects on Dynamic Response of Sandwich Structures Exposed to Underwater and In-Air Explosions", Journal of Ship Research, Vol. 51, No. 2, June 2007, pp. 83–93

15. Liviu Librescu, Sang-Yong Oh and Joerg Hohe, "Dynamic response of anisotropic sandwich flat panels to underwater and in-air explosions", International Journal of Solids and Structures 43 (2006) 3794–3816
16. Shin, Y. S., "Ship Shock Modeling and Simulation for Far-field Underwater Explosion," Computers & Structures, 82 (2004) 2211-2219.
17. Z Zong, K Y Lam, "The Flexural Response of a Submarine Pipeline to an Underwater Explosion Bubble", Journal of Offshore Mechanics and Arctic Engineering 122(2000) 194-199
18. N.K. Gupta, Pawan Kumar and S Hegde, "On deformation and tearing of stiffened and un-stiffened square plates subjected to underwater explosion — a numerical study", International Journal of Mechanical Sciences, Vol 52, Issue 5, Pp 733-744, May 2010.
19. G. I. Taylor. The pressure and impulse of submarine explosion waves on plates. In G.K. Batchelor, editor, The scienti_c papers of Sir Geo_rey Ingram Taylor,volume III: Aerodynamics and the Mechanics of Projectiles and Explosions, pages 287{303. Cambridge University Press, 1963.
20. H. Huang. Transient bending of a large elastic plate by an incident spherical pressure wave. Journal of Applied Mechanics, pages 772{776, September 1974.
21. H. Huang and Y. F. Wang. Transient interactions of spherical acoustic waves and cylindrical elastic shells. Journal of the Acoustical Society of America, 48:228{235, 1970}.
22. American Society of Civil Engineers. The Pentagon building performance report, 2003.
23. Michael F. Ashby, Anthony Evans, Norman A. Fleck, Lorna J. Gibson, John W Hutchinson, and Haydn N. G. Wadley. Metal Foams. Butterworth Heinemann,2000.
24. Joseph S. Gondusky and Michael P. Reiter. Protecting military convoys in Iraq: An examination of battle injuries sustained by mechanized battalion during operation Iraqi Freedom II. Military Medicine, 170(6):546{549, 2005.
25. Maria A. Mayorga. The pathology of primary blast overpressure injury. Toxicology, 121:17{28, 1997.
26. Zhenyu Xue and John W. Hutchinson. Preliminary assessment of sandwich plates subject to blast loads. International Journal of Mechanical Sciences, 45:687{705, 2003.

27. Zhenyu Xue and John W. Hutchinson. A comparative study of impulse-resistant metal sandwich plates. International Journal of Impact Engineering, 30:12831305, 2004.
28. V. S. Deshpande and N. A. Fleck. One-dimensional response of sandwich plates to underwater shock loading. Journal of Mechanics and Physics of Solids,53:2347-2383, 2005.
29. N. A. Fleck and V. S. Deshpande. The resistance of clamped sandwich beams to shock loading. Journal of Applied Mechanics, 71:386{401, May 2004.
30. N. A. Fleck and V. S. Deshpande. Closure to \Discussion of `The resistance of clamped sandwich beams to shock loading' " (2005, ASME J. Appl. Mech., 72, pp. 978-979). Journal of Applied Mechanics, 72:980, November 2005.
31. X. Qui, V. S. Deshpande, and N. A. Fleck. Finite element analysis of the dynamic response of clamped sandwich beams subject to shock loading. European Journal of Mechanics, 22:801{814, 2003.
32. X. Qui, V. S. Deshpande, and N. A. Fleck. Dynamic response of a clamped circular sandwich plate subject to shock loading. Journal of Applied Mechanics, 71:637-645, September 2004.
33. H. J. Rathbun, D. D. Radford, Z. Xue, M. Y. He, J. Yang, V. Deshpande, N. A. Fleck, J. W. Hutchinson, F. W. Zok, and A. G. Evans. Performance of metallic honeycomb-core sandwich beams under shock loading. International Journal of Solids and Structures, 43:1746{1763, 2006.
34. M. T. Tilbrook, V. S. Deshpande, and N. A. Fleck. The impulsive response of sandwich beams: analytical and numerical investigation of regimes of behavior. Journal of Mechanics and Physics of Solids, 54:2242{2280, 2006.
35. V. S. Deshpande and N. A. Fleck. One-dimensional response of sandwich plates to underwater shock loading. Journal of Mechanics and Physics of Solids, 53:2347-2383, 2005.
36. John W. Hutchinson and Zhenyu Xue. Metal sandwich plates optimized for pressure impulses. International Journal of Mechanical Sciences, 47:545-569, 2005.
37. Timon Rabczuk, Esteban Samaniego, and Ted Belytschko. Simplified model for predicting impulsive loads on submerged structures to account for fluid-structure interaction. International Journal of Impact Engineering, 34:163-177, 2007.

38. Douglas T. Queheillalt and H. N. G. Wadley. Cellular metal lattices with hollow trusses. Acta Materialia, 53:303-313, 2005.
39. Douglas T. Queheillalt and H. N. G. Wadley. Pyramidal lattice truss structures with hollow trusses. Material Sciences and Engineering A, 397:132-137, 2005.
40. H. N. G. Wadley, Norman A. Fleck, and Anthony G. Evans. Fabrication and structural performance of periodic cellular metal sandwich structures. Composites Science and Technology, 63:2331-2342, 2003.
41. S. C. K. Yuen and G. N. Nurick. Experimental and numerical studies of the response of quadrilateral stiffeened plates. Part I: Subjected to uniform blast load. International Journal of Impact Engineering, 31:55-83, 2005.
42. D. D. Radford, N. A. Fleck, and V. S. Deshpande. The response of clamped sandwich beams subjected to shock loading. International Journal of Impact Engineering, 32:968-987, 2006.
43. V. S. Deshpande, A. Heaver, and N. A. Fleck. An underwater shock simulator. Proceedings of the Royal Society A, 462:1021-1041, 2006.
44. T. Rabczuk, J. Y. Kim, E. Samaniego, and T. Belytschko. Homogenization of sandwich structures. International Journal for Numerical Methods in Engineering, 61:1009-1027, 2004.
45. G. S. Langdon and G. K. Schleyer. Inelastic deformation and failure of profiled stainless steel blast wall panels. Part III: Finite element simulations and overall summary. International Journal of Impact Engineering, 31:988-1012, 2005.
46. A. Vaziri, Z. Xue, and J. W. Hutchinson. Metal sandwich plates with polymer foam- filled cores. Journal of Mechanics of Materials and Structures, 1:97-127,2006.
47. M. D. Theobald and G. N. Nurick. Numerical investigation of the response of sandwich panels subject to blast loads. In M. Alves and N. Jones, editors, Impact Loading of Lightweight Structures, pages 521{534. WIT Press, Southampton, The United Kingdom, 2005.